



THE UNIVERSITY *of* EDINBURGH

## Edinburgh Research Explorer

### **Investigation of the role of bulk properties and in-bed structure in the flow regime of buoyancy-dominated flame spread in porous fuel beds**

**Citation for published version:**

Campbell-Lochrie, Z, Walker-Ravena, C, Gallagher, M, Skowronski, N, Mueller, E & Hadden, R 2020, 'Investigation of the role of bulk properties and in-bed structure in the flow regime of buoyancy-dominated flame spread in porous fuel beds', *Fire Safety Journal*. <https://doi.org/10.1016/j.firesaf.2020.103035>

**Digital Object Identifier (DOI):**

[10.1016/j.firesaf.2020.103035](https://doi.org/10.1016/j.firesaf.2020.103035)

**Link:**

[Link to publication record in Edinburgh Research Explorer](#)

**Document Version:**

Peer reviewed version

**Published In:**

Fire Safety Journal

**General rights**

Copyright for the publications made accessible via the Edinburgh Research Explorer is retained by the author(s) and / or other copyright owners and it is a condition of accessing these publications that users recognise and abide by the legal requirements associated with these rights.

**Take down policy**

The University of Edinburgh has made every reasonable effort to ensure that Edinburgh Research Explorer content complies with UK legislation. If you believe that the public display of this file breaches copyright please contact [openaccess@ed.ac.uk](mailto:openaccess@ed.ac.uk) providing details, and we will remove access to the work immediately and investigate your claim.



# Investigation of the role of bulk properties and in-bed structure in the flow regime of buoyancy-dominated flame spread in porous fuel beds

Zakary Campbell-Lochrie<sup>a\*</sup>, Carlos Walker-Ravena<sup>a</sup>, Michael Gallagher<sup>b</sup>, Nicholas Skowronski<sup>c</sup>, Eric V. Mueller<sup>a</sup>, Rory M. Hadden<sup>a</sup>

<sup>a</sup>The University of Edinburgh, Edinburgh, UK, [Z.Campbell.Lochrie@ed.ac.uk](mailto:Z.Campbell.Lochrie@ed.ac.uk)

<sup>b</sup>USDA Forest Service, Northern Research Station, New Lisbon, New Jersey, USA

<sup>c</sup>USDA Forest Service, Northern Research Station, Morgantown, West Virginia, USA

\*Corresponding author

## Abstract:

In a quiescent atmosphere, the flame spread process in porous fuels is controlled to a large degree by the fuel bed structure, fuel loading and bulk density, and fuel moisture content. Previous studies have shown that increases in flame spread rate, fire intensity and burning rate are observed with independent increases in fuel loading or decreases in bulk density, however neither of these parameters adequately describe the physical processes that control flame spread. A series of laboratory-based, flame spread experiments involving fuel beds of differing fuel loading and structure were conducted in the absence of wind and slope effects and with consistent fuel conditioning. Changes in fuel bed structure are shown to change the observed fire behavior in both the flaming phase and the smouldering region behind the flame front, while also influencing the physical mechanisms contributing to flame spread. Bulk density and fuel loading were shown to independently affect the physical mechanisms both above (buoyant flow regime) and within (in-bed flow, gas phase temperature) the fuel bed. Increases in buoyant flow velocity were observed with increases in fuel loading, along with increases in the maximum in-bed entrainment induced towards the approaching flame front. To fully understand the complex interlinking of these flow regimes and their role in quiescent flame spread, physically linked parameters to describe the internal fuel bed structure must be developed.

**Keywords:** flame spread, fuel structure, in-bed flow, porous fuels, low-intensity fires, buoyant flow

## Nomenclature

$c_p$	specific heat (kJ/kg.K)
$D$	Combustion Region Depth (m)
$g$	Gravitational Acceleration (m/s <sup>2</sup> )
$I$	Fireline Intensity (kW/m <sup>2</sup> )
$N_c$	Byram Convective Number
$T$	Temperature (K)
$U_w$	Ambient Wind Speed (m/s)
$V_f$	Spread Rate (m/s)
$v$	Velocity (m/s)
$\alpha$	Porosity (Gaseous Volume Fraction)
$\beta$	Packing Ratio
$\delta$	Fuel Bed Height (m)
$\lambda$	Porosity (Void Volume : Total Fuel Surface Area)
$\rho$	Density (kg/m <sup>3</sup> )
$\rho^*$	Bulk Density (kg/m <sup>3</sup> )
$\sigma$	Surface-to-Volume Ratio (m <sup>-1</sup> )

## 1. Introduction

Laboratory studies of flame spread in natural porous fuel beds have generally focused on the effect of environmental, topographical and fuel conditions on the flame spread in wildland fire scenarios. The effect of upward [1,2] and downward slope angles [3,4], complex topographical features [5], and Fuel Moisture Content (FMC) [6] have been investigated. While wind tunnel experiments have studied the role of both concurrent [7,8] and opposed wind flow [4,9].

Studies focused on fuel properties have typically focused on manipulating the fuel load or bulk density [10,11], individual fuel element properties [6,12], or FMC [13]. These studies have consistently demonstrated a positive relationship between fuel loading and flame spread rate and a negative relationship between spread rate and bulk density. Similarly, spread rate damping coefficients have been proposed to account for moisture and mineral content, while the underlying physical effects of FMC in the flame spread process have been investigated numerically and experimentally [13]. Studies focused on fuel bed structure have generally reduced the complexity of the problem, by simplifying the fuel structure by using well-defined fuel beds composing uniform engineered materials (sticks, laser-cut cardboard, wood cribs), or by reducing the influence of wind and slope by studying natural fuels in a quiescent (no flow) atmosphere [11,12,14]. Nevertheless, there remains a need for quantitative analysis of the physical processes introduced by the fuel bed structure which underpin the observed changes in flame spread rate.

### 1.1 Opposed Flow Flame Spread

Opposed flow flame spread describes a regime in which the flame spread direction is in the opposite direction to the lateral air flow. In the absence of wind, flame spread can also occur in quiescent (no flow) conditions, in which the importance of terrain and fuel properties will be emphasised.

Under conditions of low or no wind, the buoyancy force of the plume is greater than the inertia of the wind. The ratio between these two competing forces can be expressed through the dimensionless Froude number or, in the context of wildland fires, in terms of the Convective Byram Number ( $N_c$ ) [15] in which the ratio expressed is the resulting power of each of the two forces. This is calculated through the inclusion of terms for ambient wind ( $U_w$ ), rate of spread ( $V_f$ ) and fireline intensity ( $I$ ).

$$N_c = \frac{2gI}{\rho c_p T_0 (U_w - V_f)^3}$$

From this formulation, two distinct flame spread regimes have been defined, wind dominated flame spread ( $N_c \ll 1$ ), and plume dominated flame spread when  $N_c \gg 1$ .

For quiescent conditions, the resulting flame spread is therefore characteristically in the plume dominated regime. Given the lack of ambient wind flow, the only lateral flow will be the fire-induced entrainment, driven by the buoyant flow. Ahead of the travelling flame front, air will be entrained towards the flame front hence the fire-induced flow will be in the opposite direction to the flame travel direction. This therefore allows comparison between quiescent and opposed flow regimes, in which the wind flow direction is also the reverse of the flame travel direction.

In opposed flow flame spread, the magnitude of the airflow to the combustion zone will dictate the rate of flame spread and the dominant heat transfer mechanism. Under quiescent

conditions, the magnitude of the entrained flow is controlled by the Heat Release Rate (HRR) of the fire, which in turn is controlled by the fuel structure as this dictates the heat and mass transfer conditions. This feedback loop has been studied previously in non-porous fuels (particularly continuous solids and pool fires) [16,17] however with a porous fuel the entrained air may pass over the surface or through the fuel bed. This will impact on the dominant mode of heating. While there have been attempts to model the fire induced flow involved in porous flame spread [18], there is a lack of experimental quantification of this fire-induced flow, which is required for further validation and development of the sub-models used in physical models. This is particularly true of the in-bed flow region (which is affected by the internal porous bed structure), with past experimental studies of entrained flow focusing on flow above the fuel bed [19,20].

Furthermore, the use of porous structures changes the characteristic length scales of the problem from those typically observed in non-porous solid fuels. For continuous solid fuels, in simple terms, an energy balance can be applied to the solid surface (encompassing all heat transfer from above the fuel to the surface). The dominant form of energy transfer through the solid can be assumed to be in the form of conduction, with distinction drawn between thermally thick and thin fuels [21]. For a porous fuel bed however, given the surface porosity, there is clearly heat transfer from above the bed through the depth of the fuel bed. Similarly, the assumption of conduction driven heat transfer through the fuel bed is complicated by the highly porous structure which introduces radiative and convective heat transfer within the fuel bed. Additionally, the flow of ambient entrained air through the fuel bed will affect the convective cooling of the fuel, which if increased may increase the time to ignition of individual fuel elements [22].

In the absence of wind or slopes, the above-bed flame is typically upright or slightly backwards tilting resulting in a small view factor between the flame and the unburned fuel. This adds additional importance to the understanding of heat transfer through the fuel bed, leading to past authors [7,23] to consider an idealised combustion zone of homogeneous fuel elements, of a given height ( $\delta$ ) and depth ( $D$ ), with a free flame attached at the surface and moving at a rate of spread ( $V_f$ ) at a given air velocity  $U_a$ . The flow into this combustion region will also affect heat release from both the flaming and smouldering combustion phases, with both phases contributing to the overall heat release (and hence fire intensity).

Consequently, in order to describe the effect of the fuel bed structure on the flame spread rate, it is necessary to evaluate the flow profile as a function of fuel structure. The structure of the fuel bed will determine the parameters which affect the air flow (permeability and drag) which in turn will change the dominant heat transfer mechanisms. The overall flame spread behaviour will therefore be a function of fuel bed structure, as a result of changes to convective heat transfer, oxygen availability, radiation attenuation and char oxidation rate.

## 1.2 Porous Fuel Bed Structure

The porous fuels typical of wildland fire spread are permeable to air, and the influence of this oxidiser flow on the combustion processes and the underlying physical mechanisms must be understood. Previous studies have focused mainly on the effect of overall fuel bed structure, characterised in the form of fuel loading, bulk density ( $\rho^*$ ), packing ratio ( $\beta$ ), and fuel bed height ( $\delta$ ) [11,24], with some additional consideration of individual element properties such as surface-to-volume ratio ( $\sigma$ ), characteristic length and density ( $\rho$ ) [6,25].

From the existing literature on flame spread experiments conducted in quiescent conditions, several trends have emerged. These have generally indicated that an increase in fuel loading results in an increased rate of flame spread, along with increasing mass loss rate, flame height

and HRR or fire intensity, with similar trends observed for decreases in bulk density [24,26]. For certain fuel types, a trend of increasing flame spread rate and HRR with increasing fuel bed height has also been indicated for cases where fuel loading is kept constant [27] and those where bulk density is kept constant [11,24].

Despite these identified links between fuel bed structure and fire behaviour, there presently exists no complete understanding or theory of fire spread in porous fuel layers. Furthermore, many of the parameters commonly used to describe the fuel bed do not directly relate to the physical processes which control the phenomenon. In addition, it is clear that this is a multiscale problem and that components of the fuel element scale and the global fuel bed structure will be relevant.

It is important that parameters describing the porous internal structure of the fuel bed are related to actual physical mechanisms if their role in the flame spread process is to be understood. Certain dimensionless parameters for the burning of porous fuels have previously been suggested, particularly in the context of engineered materials (cribs, sticks and excelsior) [12,26]. Rothermel and Anderson [6] suggested the use of  $\sigma\lambda$ , where  $\lambda$  is the porosity, defined by those authors as the fuel bed void volume divided by the total surface area of fuel in the bed. This parameter is therefore analogous to the ratio of porosity (defined as the volume fraction,  $\alpha$ ) and the packing ratio ( $\beta$ ).

Meanwhile, Wilson [12], and later Anderson [28], related the optical density of the fuel bed  $\sigma\beta$  to the surface area burning rate. This later work drew heavily on the existing literature for crib fires, for which two regimes have commonly been proposed, a ventilation controlled regime (when fuel elements are closely packed) and an exposed fuel surface area regime (when fuel elements are loosely packed). For both regimes it has been suggested that the mass loss per unit area of fuel surface can be described as a function of the ventilation area to exposed fuel surface area (porosity factor) [12]. Application to a wildland fuel bed context must however consider the influence of potentially greatly differing aspect ratios and the characteristically thin elements in, for example pine needle fuel beds, as well as the role of the ground beneath the bed as a boundary condition, and limit to entrainment [29].

In order to characterise the effects of fuel structure on the processes which control flame spread, an experimental programme was designed that allowed the effect of fuel bed characteristics on the fluid flow to be explored systematically and the relevant phenomena to be measured. The effects considered in this study concerns flame spread on a porous (pine needle) fuel bed in a quiescent environment (no wind, no slope). The experimental method used is outlined in detail, followed by observations of the resulting fire behaviour (spread rate, flame height, fire line intensity) of fuel beds of varying structure. This is compared with identified trends from existing studies for commonly used descriptors of wildland fuel beds (fuel loading, bulk density, bed height). Physical observations above (buoyant velocity) and within the fuel bed (in-bed temperatures, in-bed flow) are then examined to explore the adequacy of these descriptors as predictors of fire behaviour and their relation to the physical mechanisms controlling this fire behaviour.

## 2. Material and Methods

Fuel beds were constructed on a 1.5 m x 0.67 m flame spread table (the Table), with a vermiculite substrate base. Steel sidewalls, covered with alumina-silica fibre, were adjusted to a height of 0.03 m above the fuel bed surface. This limits lateral entrainment into the fuel bed which has been shown to promote a more linear flame front [30]. The Table was situated under a furniture calorimeter allowing the energy release rate to be measured using oxygen

consumption calorimetry [31], assuming an energy release value per unit of  $O_2$  consumed of 14.15 kJ/g $O_2$ , as determined for forest fuels by Bartoli [32].

## 2.1 Flame Spread Table Instrumentation

The Table was instrumented in three locations (0.5 m, 0.8 m and 1.1 m from the ignition line, in the direction of the fire spread) as shown in Fig. 1. Flow in the bed was measured at a height of 10 mm above the base of the table. Flow measurements were derived from measurements using bi-directional pressure probes (20 mm probe diameter) and a gas phase thermocouple (0.25 mm, K Type) [33].

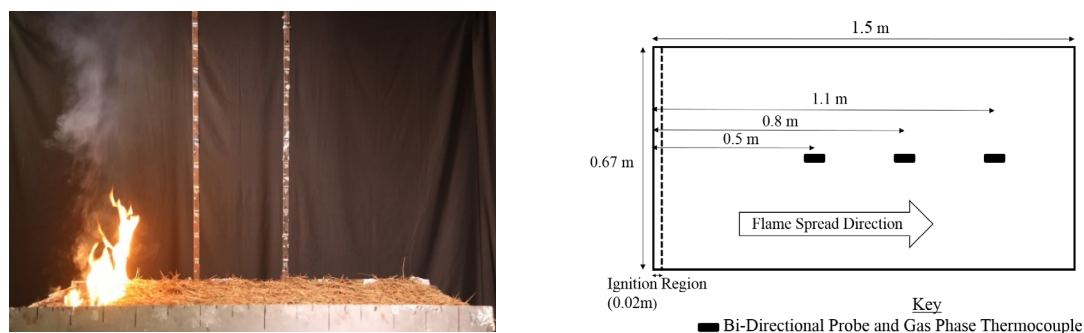


Fig. 1. Photograph and schematic of the Table, detailing the position of in-bed bi-directional pressure probes and gas phase thermocouples (all measurements at a height of 0.01 m above the vermiculite substrate surface)

For a subset of experiments, additional pressure probes (and accompanying gas phase thermocouples) were also positioned vertically at a height of 1.2 m above the fuel bed at the first two measurement locations (0.5 m and 0.8 m from the ignition line) to measure the upward (buoyant) velocity above the fuel bed.

For every experiment, ignition was in the form of a line ignition at one short edge of the table using a 0.67 m long strip of alumina-silica fibre, on which 10 ml of acetone was distributed. This was observed to result in the formation of a linear front immediately after ignition in all but the lowest fuel loadings (0.2 kg/m<sup>2</sup>). The average burning duration of this ignition line was 61 seconds (maximum 69 seconds). Both overhead and side-on (perpendicular to flame travel direction) video footage was recorded throughout the experimental duration.

The in-bed temperatures were used to calculate the residence time at each thermocouple location, using a temperature threshold of 300 °C. The same threshold value was used to calculate the arrival time of the flame front at each pressure probe. The flame spread rate was calculated through video analysis of the flame front position over time. An arrival time was determined, based on the leading edge of the front centreline, at 0.1 m distances from the ignition line. Regression analysis was used to determine the spread rate, with the standard deviation in spread rate across all 0.1 m table segments also calculated.

Flame heights were determined through video analysis, with a vertical length scale (0.05 m divisions) aligned with the measurement locations, as shown in Fig. 1. The flame height was defined as the distance between the fuel bed surface and the peak of the continuous flame region [34]. Additional analysis of the visual imagery allows additional qualitative analysis of the flame front shape and depth, and the smouldering combustion region.

## 2.2 Fuels and Conditioning

The fuel beds for each experiment consisted solely of dead pine needles, with two separate experimental series completed, each using a different needle species. The two needle types

used were *Pinus rigida* (Pitch Pine) and *Pinus rigida x taeda* (Pitch - Loblolly Pine hybrid). Both needle species were collected in the Silas Little Experimental Forest, New Lisbon, New Jersey [35].

Needles were air-dried in a storage room and otherwise unconditioned prior to experiments. The FMC was measured for each experiment, by drying ~20 g samples of pine needles in an oven for 24 hours at 60 °C [36]. The bomb calorimeter was used to measure the high heat of combustion of each species as given in Table 1. The individual needle geometrical properties, including the surface-to-volume ratio ( $\sigma$ ) were measured through random sampling, using the methods outlined by Thomas *et al.* [37]. The average FMC (dry basis) for each needle type is also given, with the FMC higher across the Pitch-Loblolly Pine hybrid series, than those involving the Pitch Pine needles.

Table 1. Needle for *Pinus rigida* and *Pinus rigida x taeda* needles species

Species	Mean Density, $\rho$ [kg/m <sup>3</sup> ] (SD)	Mean Needle Diameter [mm] (SD)	Mean Surface to Volume Ratio, $\sigma$ [m <sup>-1</sup> ] (SD)	Average Fuel Moisture Content [% Dry] (SD)	High Heat of Combustion [kJ/kg] ( $\pm$ Max-Min)
<i>Pinus rigida</i> (Pitch Pine)	706 (71)	1.31 (0.15)	5063 (640)	10.1 (0.8)	19669 $\pm$ 422
<i>Pinus rigida x taeda</i> (Pitch-Loblolly Pine)	725 (33)	1.34 (0.12)	4899 (446)	16.0 (0.9)	19672 $\pm$ 346

The fuel bed was constructed by randomly dropping (without controlling the orientation or final needle position) the needles on to the Table. To achieve a uniform fuel loading and bed height, the Table was divided into 10 equally sized segments and 10 % of the total fuel load was loaded onto each segment. After the fuel bed was constructed, the average height was randomly measured at ten locations, to ensure the desired average height was achieved.

Across tests, the fuel loading of the fuel bed was varied (0.2 kg/m<sup>2</sup>, 0.4 kg/m<sup>2</sup>, 0.6 kg/m<sup>2</sup>, 0.8 kg/m<sup>2</sup>, 1.2 kg/m<sup>2</sup>, 1.6 kg/m<sup>2</sup>) on a wet basis. The fuel bed bulk density ( $\rho^*$ ) was altered (10 kg/m<sup>3</sup>, 20 kg/m<sup>3</sup>, 40 kg/m<sup>3</sup>) by varying the fuel bed height ( $\delta$ ) for fuel beds of constant fuel loading. Replicate experiments were conducted for each fuel bed case, given the potential for heterogeneity within the fuel bed structure.

For the highest bulk density tests (40 kg/m<sup>3</sup>), compression of the fuel bed was required to achieve the desired fuel bed height. The fuel bed porosity,  $\alpha$  was calculated using the packing ratio  $\beta$ ,

$$\alpha = 1 - \beta \quad (3)$$

The porosities of the fuel beds for the different experimental conditions are given in Table 2 and Table 3, along with the average FMC for each case.

### 3. Results and Analysis

Significant variations in fire behavior were observable as the fuel loading and bulk density of the fuel bed were varied. Fig. 2 shows the fire front characteristics and times of flame front arrival at each measurement location for pitch pine fuel beds. It can be observed that the spread rate and flame height increased with increasing fuel load and for decreasing bulk density. At fuel loadings of 0.4 kg/m<sup>2</sup> or higher, the flame front was observed to be continuous across the width of the fuel bed. At the lowest fuel loading (0.2 kg/m<sup>2</sup>) the flame



front became discontinuous with flame spread between individual needles and clusters appearing to dominate.

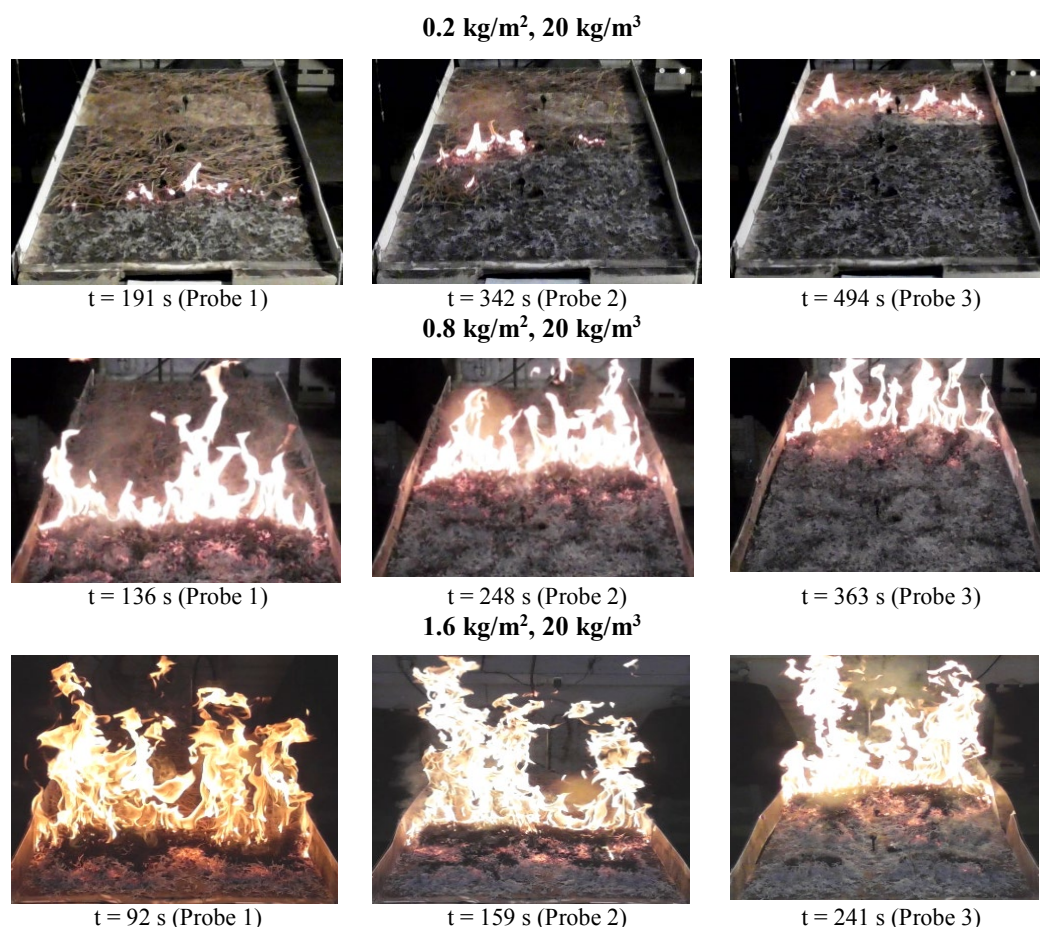


Fig. 2. Composite of frames from downward-looking video footage of flame spread experiments displaying variation in flame and front shape between Pitch Pine fuel beds of (Top)  $0.2 \text{ kg/m}^2$ ,  $20 \text{ kg/m}^3$  (Middle)  $0.8 \text{ kg/m}^2$ ,  $20 \text{ kg/m}^3$  (Bottom)  $1.6 \text{ kg/m}^2$ ,  $20 \text{ kg/m}^3$ .

Key fire behaviour measurements for all experiments are summarised in Table 2 for the Pitch Pine fuel beds and in Table 3 for those involving Pitch-Loblolly Pine hybrid needles. For these measurements, the mean values across repetitions are reported for each fuel bed case. The mean spread rate was calculated based on continuous 0.1 m segments in all experiments, while the mean of the HRR was calculated based on the steady state period across all experiments at a given fuel bed condition. The mean residence time for all in-bed thermocouples was calculated, with the average for each fuel bed condition reported.

For both species, the flame spread rate, peak HRR and flame height increased with independent increases in fuel loading or decreases in bulk density, in agreement with the previously discussed trends in the existing literature [11,24,26].

The importance of the small scale (inter-needle) variations in structure was also observed in the Pitch-Loblolly Pine hybrid experimental series. For this needle species, fuel beds of  $0.2 \text{ kg/m}^2$  and 16.6 % moisture content were unable to sustain flame spread across the entire Table, however the distance from the ignition line at which extinction occurred varied between repeat experiments.



While a positive linear trend was observed between fuel loading and residence time for the hybrid needles ( $R^2 = 0.99$  for 20 kg/m<sup>3</sup> fuel beds), in the case of the pitch pine needles, following an initial linear correlation, a peak residence time was observed at 1.2 kg/m<sup>2</sup> (for 20 kg/m<sup>3</sup> cases) and 0.6 kg/m<sup>2</sup> (for 10 kg/m<sup>3</sup> cases). Significant variations in residence times were however observed at specific fuel bed conditions, which may be due to the complex interaction of both the smouldering and flaming phases given the in-bed location of the temperature measurement. Within the fuel bed, neighbouring regions of smouldering and flaming combustion are often observed simultaneously along with transition between these phases. Based on qualitative visual analysis, at the lowest fuel loading (0.2 kg/m<sup>2</sup>) there was a notable absence of the smouldering region behind the flame front, shown in the higher fuel loading cases in Fig. 2.

Table 2. Summary of fuel bed parameters and measured fire behaviour for experiments involving Pitch Pine needle fuel beds

Fuel Loading (kg/m <sup>2</sup> )	Bulk Density, $\rho^*$ (kg/m <sup>3</sup> )	Fuel Bed Height, $\delta$ (m)	Porosity, $\alpha$	Fuel Moisture Content (% $\pm$ Std. Dev.)	Flame Spread Rate (mm/min $\pm$ Std. Dev.)	Steady State HRR (kW $\pm$ Std. Dev.)	Residence Time (s $\pm$ Std. Dev.)	Flame Height (m $\pm$ 0.025 m)
0.2	10	0.02	0.986	10.1 $\pm$ 1.1	108 $\pm$ 31	12.2 $\pm$ 3.1	17 $\pm$ 9	0.10
0.2	20	0.01	0.972	10.0 $\pm$ 1.2	114 $\pm$ 24	1.1 $\pm$ 1.1	18 $\pm$ 10	0.05
0.4	10	0.04	0.986	9.6 $\pm$ 0.8	144 $\pm$ 20	15.4 $\pm$ 1.6	20 $\pm$ 11	0.23
0.4	20	0.02	0.972	9.6 $\pm$ 0.6	126 $\pm$ 17	10.5 $\pm$ 1.5	29 $\pm$ 9	0.16
0.6	10	0.06	0.986	10.9 $\pm$ 2.1	180 $\pm$ 28	24.1 $\pm$ 3.6	30 $\pm$ 10	0.43
0.6	20	0.03	0.972	9.8 $\pm$ 0.7	132 $\pm$ 19	18.6 $\pm$ 1.8	33 $\pm$ 14	0.29
0.8	10	0.08	0.986	10.1 $\pm$ 0.5	210 $\pm$ 26	39.4 $\pm$ 2.0	27 $\pm$ 15	0.57
0.8	20	0.04	0.972	10.2 $\pm$ 0.7	162 $\pm$ 16	28.9 $\pm$ 3.6	46 $\pm$ 14	0.42
0.8	40	0.02	0.943	10.1 $\pm$ 0.9	126 $\pm$ 37	N/A	38 $\pm$ 24	0.33
1.2	20	0.06	0.972	11.3 $\pm$ 0.3	174 $\pm$ 33	N/A	64 $\pm$ 52	0.65
1.6	20	0.08	0.972	12.3 $\pm$ 1.7	246 $\pm$ 39	N/A	49 $\pm$ 23	0.93

Table 3. Summary of fuel bed parameters and measured fire behaviour for experiments involving Pitch-Loblolly Pine hybrid fuel beds

Fuel Loading (kg/m <sup>2</sup> )	Bulk Density, $\rho^*$ (kg/m <sup>3</sup> )	Fuel Bed Height, $\delta$ (m)	Porosity, $\alpha$	Fuel Moisture Content (% $\pm$ Std. Dev.)	Flame Spread Rate (mm/min $\pm$ Std. Dev.)	Steady State HRR (kW $\pm$ Std. Dev.)	Residence Time (s $\pm$ Std. Dev.)	Flame Height (m $\pm$ 0.025 m)
0.2	10	0.02	0.986	16.6 $\pm$ 1.9	Unsustained	N/A	N/A	N/A
0.2	20	0.01	0.972	16.6 $\pm$ 1.9	Unsustained	N/A	N/A	N/A
0.4	10	0.04	0.986	15.3 $\pm$ 1.2	114 $\pm$ 25	9.3 $\pm$ 2.0	28 $\pm$ 18	0.21
0.4	20	0.02	0.972	15.5 $\pm$ 0.3	90 $\pm$ 21	6.6 $\pm$ 2.1	15 $\pm$ 14	0.10
0.6	10	0.06	0.986	15.6 $\pm$ 0.3	156 $\pm$ 39	18.1 $\pm$ 2.9	37 $\pm$ 17	0.35
0.6	20	0.03	0.972	17.1 $\pm$ 0.7	114 $\pm$ 18	13.1 $\pm$ 2.5	23 $\pm$ 13	0.28
0.8	10	0.08	0.986	15.9 $\pm$ 0.6	162 $\pm$ 28	28.9 $\pm$ 3.0	45 $\pm$ 7	0.48
0.8	20	0.04	0.972	15.7 $\pm$ 2.4	126 $\pm$ 21	17.5 $\pm$ 1.6	45 $\pm$ 31	0.4
0.8	40	0.02	0.945	16.0 $\pm$ 0.8	96 $\pm$ 11	11.9 $\pm$ 1.4	29 $\pm$ 14	0.28

### 3.1 Spread Rate

The position of the flame front from the ignition line ( $x = 0$ ), versus the time from ignition was determined from video analysis. This flame front position over time is plotted in Fig. 3 for Pitch Pine fuel beds of different fuel loading and bulk density.

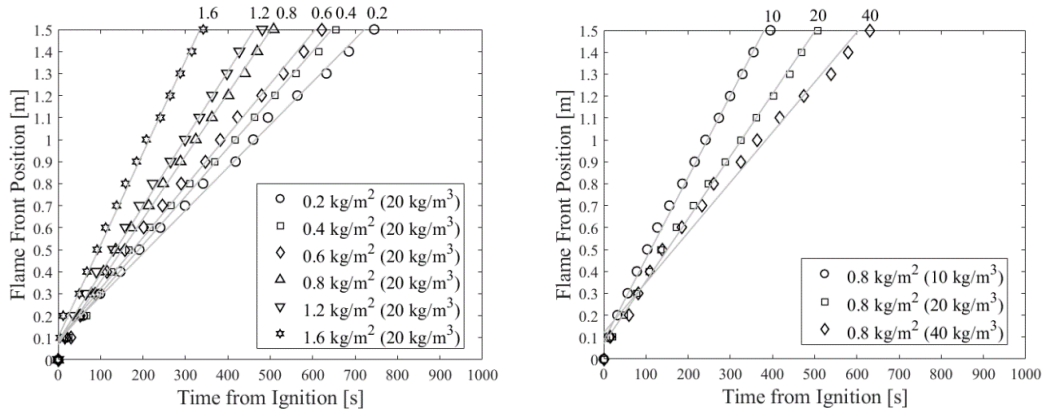


Fig. 3. Flame front position versus time from ignition for Pitch Pine beds of (a) 20 kg/m<sup>3</sup> bulk density, and (b) 0.8 kg/m<sup>2</sup> fuel loading (avg. of all experiments at each condition)

There is an apparent reduction in flame spread rate after the initial post-ignition time period (during the first 0.3 m from the ignition line) which is likely due to the influence of the ignition source. The length of this ignition affected region is similar to the maximum burning duration of the ignition source (69 s) multiplied by the maximum flame spread rate (246 mm/min) which results in a maximum flame propagation distance of 0.28 m while the ignition source is present, which is well before the first measurement location is reached.

This initial 0.3 m region was therefore not considered when deriving the flame spread velocity for each fuel bed condition using a least squares regression, with the calculated correlation coefficient ( $R^2$ ) providing an indication of the degree of linearity of the observed flame spread. The correlation coefficient was greater than 0.99 in all cases, which, in line with previous studies [38] was assumed to indicate flame spread of a quasi-steady nature.

In reality, the instantaneous flame spread rate may vary across the table due to heterogeneity in both the combustion region and the fuel bed properties. This variability is demonstrated in Fig. 4, where the flame spread rate is plotted as a function of distance from the ignition line, for each 0.1 m segment of the flame spread table (starting with the spread rate between 0.3 m and 0.4 m from the ignition line).

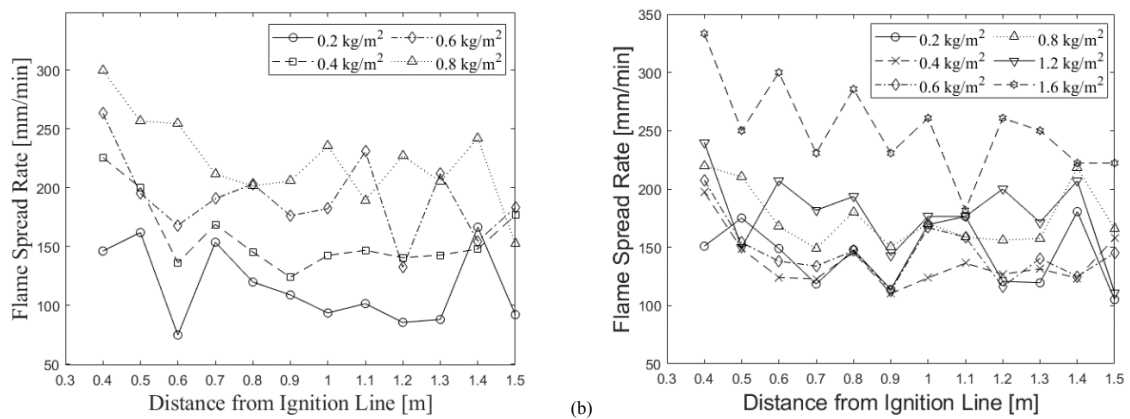


Fig. 4. Flame Spread Rate as a function of distance (based on video analysis) for Pitch Pine fuel beds of different fuel loadings at (a) 10 kg/m<sup>3</sup> bulk density, and (b) 20 kg/m<sup>3</sup> bulk density

In Table 2 and Table 3, a trend of increasing flame spread rate with increasing fuel load or decreasing bulk density respectively is observed. Neither the fuel loading nor the bulk density alone adequately describe the variation in flame spread rate, with both parameters having an

influence, as shown by the variation in spread rate for fuel beds at consistent fuel loading but differing bulk density in Fig. 5. For  $0.8 \text{ kg/m}^2$  Pitch Pine fuel beds, the spread rate increased from  $126 \pm 37 \text{ mm/min}$  for  $40 \text{ kg/m}^3$  fuel beds to  $210 \pm 26 \text{ mm/min}$  for  $10 \text{ kg/m}^3$  fuel beds. The variation in spread rate with independent changes in either bulk density or fuel loading is also demonstrated in Fig. 3 for a range of bulk densities.

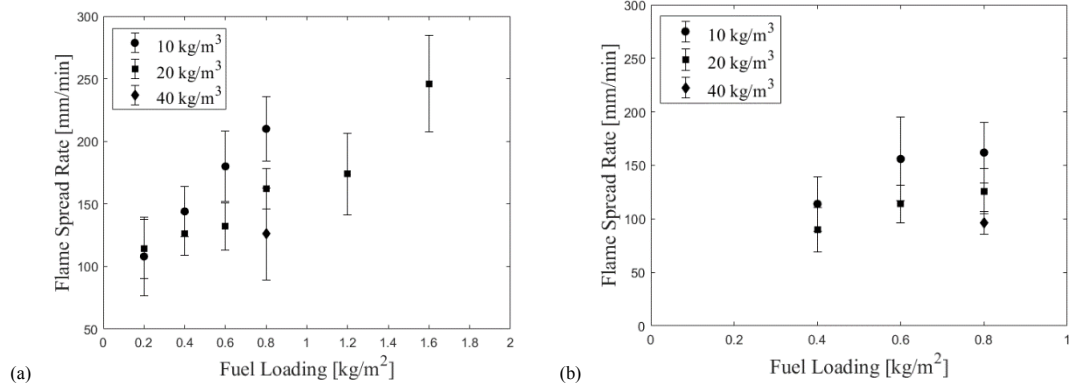


Fig. 5. Comparison of flame spread rate with fuel loading and bulk density for, (a) Pitch Pine (b) Pitch-Loblolly Pine hybrid, needle fuel beds

Examining instead the effect of fuel bed height [27,39], demonstrates a greater correlation with spread rate with a smaller observable impact of changes in either fuel loading or bulk density. This suggests that other aspects of the fuel bed structure, not adequately described by fuel loading and bulk density parameters, are significantly influencing the flame spread rate.

Comparison of the spread rate with the dimensionless fuel bed parameter  $\sigma\lambda$ , proposed by Rothermel and Anderson [6], displays a strong correlation only once normalised with respect to fuel loading. The fuel loading therefore has a multiplier effect on the original parameter  $\sigma\lambda$  similar to the way in which wind loading was originally included [6]. Normalisation in this manner however loses the dimensionless property inherent in this original descriptor.

Given that the Rothermel and Anderson term for porosity  $\lambda$ , is defined as the ratio of void volume to surface area of fuel in the bed, the parameter  $\sigma\lambda$  can also be considered in terms of packing ratio as  $\frac{1-\beta}{\beta}$ , therefore multiplication by the packing ratio ( $\beta$ ), surface-to-volume ratio of fuel elements ( $\sigma$ ), and the fuel bed height ( $\delta$ ) results in an alternative dimensionless parameter  $\alpha\sigma\delta$ , where  $\alpha$  is the fuel bed porosity. The correlation of  $\alpha\sigma\delta$  with flame spread rate is shown in Fig. 6, and this parameter can be considered in terms of a porosity factor.

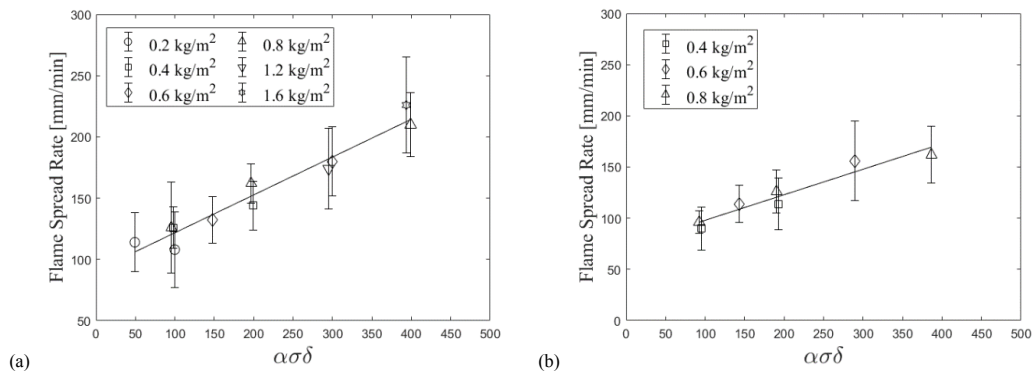


Fig. 6. Correlation between  $\alpha\sigma\delta$  and flame spread rate in (a) Pitch Pine (b) Pitch-Loblolly Pine fuel beds

The  $\alpha\sigma\delta$  term is similar to the bed descriptor  $\beta\sigma\delta$  introduced by Wilson [12], and later Anderson [28], based on the optical depth term  $\sigma\beta$ . Using that parameter, a constant value can be obtained for fuel beds of identical fuel loading but different bulk density, where the height is altered (due to cancellation of the  $\beta$  and  $\delta$  terms). In this study however variation in spread rate and fire behaviour were observed for fuel beds of equal fuel loading but differing bulk density.

Additionally the porous fuel beds described in this study are quite different structurally to excelsior and wooden cribs. The fuel beds used by Anderson, for example were significantly less porous than those here, however this is due to differing element properties ( $\sigma, \rho$ ) in addition to changes to the pore structure, the combined effect of which must be further explored to understand the relative merit of different structural parameters in a given scenario.

Used in this study, the proposed  $\alpha\sigma\delta$  allows independent influences from both bulk density and fuel loading changes to be incorporated. As with past studies however, this parameter has been investigated only at the range of structural conditions described in this study. Further investigation of the effect of variation in  $\sigma$  using different fuel types should be explored.

To understand these changes in flame spread, the role of the fuel bed properties within the feedback loop between the increasing HRR, flame height (and the associated changes to the buoyant flow regime) and the resulting entrainment profile into the combustion region must be investigated.

## 3.2 Flows

At quiescent conditions (and in the absence of a slope), the buoyant plume above the combustion zone is expected to result in entrainment towards the combustion region. The entrainment flow profile will rely not only on the magnitude of the buoyant flow but also on the internal porous fuel bed structure, which may alter the drag and flow regimes. The effect of this structure on entrainment into the combustion region will modify the heat transfer and oxygen supply in both the flaming and smouldering phases.

### 3.2.1 Buoyant Flow

The buoyant flow profile above the flame fronts of different fuel beds was compared across a 10 s window following the arrival of the flame front underneath the above-bed pressure probe. This interval was chosen to allow proper characterisation of the average plume features, while avoiding periods in which the flame front was no longer present (based on the minimum measured residence time of 17 s).

The pressure probes were at a height of 1.2 m above the table surface. While this height is constant with respect to the table surface, the height relative to the flame tip varies. Although the measurement is always upstream of the flame tip (in the buoyant plume region) with the focus on comparison of the overall buoyant system. The velocity is reported relative to the average pre-experiment velocity (measured in the 1 minute period prior to ignition) which characterises the background velocity profile.

During the post-flame arrival period, an increased maximum buoyant flow above the fuel bed was observed with increasing fuel load as shown in Fig. 7, with the peak buoyant flow increasing from 1.3 m/s to 2.6 m/s, as the fuel loading was increased from 0.2 kg/m<sup>2</sup> to 0.8 kg/m<sup>2</sup>.

Fig. 7 also shows that a slight variation in maximum buoyant flow velocity as the bulk density decreases from 20 kg/m<sup>3</sup> to 10 kg/m<sup>3</sup> at a fuel loading of 0.6 kg/m<sup>2</sup>. The opposite effect however is observed for fuel beds of fuel loading of 0.4 kg/m<sup>2</sup> or lower.

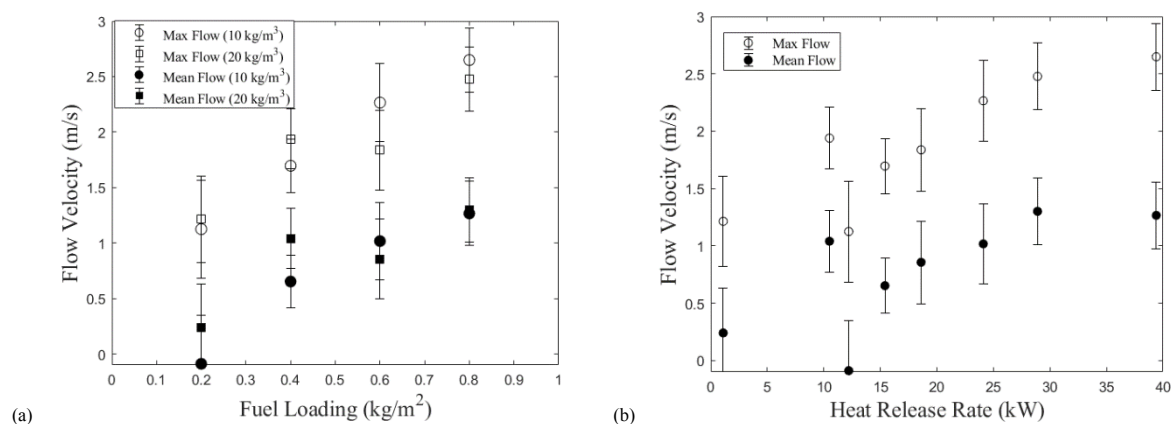


Fig. 7. Comparison of (a) Fuel Loading, (b) Heat Release Rate with mean and max. buoyant flow velocity at a height of 1.2 m above Pitch Pine fuel bed, in the 10 s after flame arrival

The increasing maximum buoyant flow velocity with increasing fuel loading matches the observed trend in past Particle Image Velocimetry (PIV) based studies of the buoyant flow profile above excelsior fuel beds (no wind, no slope conditions) [19]. As expected, there is also largely a positive trend between HRR and both the mean and maximum vertical flow magnitudes as shown in Fig. 7b. The lowest HRR values in Fig. 7b correspond to the 0.2 kg/m<sup>2</sup> fuel beds and for these cases increased variation may be expected given the discontinuous, non-linear nature of the flame front.

### 3.2.2 Buoyancy Induced Flows

The buoyant upward flow results in lateral entrainment of air, and as such, an opposed flow flame spread regime. This pattern of entrainment, firstly towards the approaching flame front and then reversing towards the departing flame front is observed in this study, in a similar manner to studies of above bed, lateral flow [20].

The magnitude of the entrainment towards the approaching flame front, through the intact, unburned fuel structure, was compared across fuel bed types. This was calculated by investigating the flow profile over a distance of 50 mm to 10 mm between the probe and the approaching flame front, prior to flame arrival.

This period was chosen through observation of the flow profile across all tests, where the onset of the measurable entrainment occurred at a distance of around 50 mm ahead of the flame. The use of a 10 mm cut-off reduces the influence of any local flame impingement, structural changes in the fuel bed, or flow reversal ahead of the recorded flame arrival time. During this period negative flow indicates flow towards the approaching flame front, and therefore characterises the fire-induced entrainment.

Both the minimum and mean flow velocities were calculated, and as shown in Fig. 8 an overall trend of increasing mean entrainment velocity is observed with increasing fuel loading (and hence HRR), however the 1.2 kg/m<sup>2</sup> pitch pine fuel bed is an exception to this observed trend. At the highest fuel loadings (1.2 kg/m<sup>2</sup> and 1.6 kg/m<sup>2</sup>) greater variation in both mean and peak entrainment velocity values were recorded, as demonstrated by the larger (max-min) error bars in Fig. 8. Additionally at these highest fuel loadings, the peak velocity (in the

opposite direction to the flame travel direction) was in some cases observed after flame arrival (and was therefore outside of the window considered in Fig. 8). Further investigation is required to separate the influence of the increased spread rate from the possible physical effects based on the flame dynamics and fuel bed structure. Bulk density also appears to affect the entrainment flow, with variation in mean entrainment flow observed for fuel beds of equal fuel loading. The increase in bulk density is, as shown earlier, accompanied by a decrease in HRR.

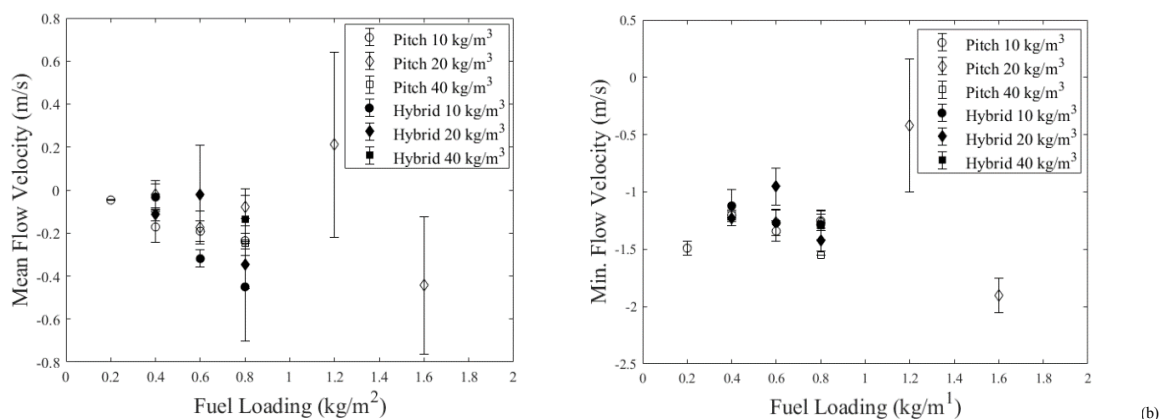


Fig. 8. Mean and minimum in-bed flow velocity towards the approaching flame front (50 mm to 10 mm prior to flame arrival), in beds of different fuel loading and bulk density for beds of Pitch Pine and Pitch-Loblolly Pine hybrid respectively

Interestingly, these observed trends are less clear for the minimum flow velocities, which may reflect the highly transient nature of the flow. As well as the effect of both local fuel structure variations and fine scale variations in the local buoyant flow profile as a result of variations in bed structure (pore size, connectivity and permeability varies).

If the air being entrained towards the approaching flame front is assumed to be ambient air, then any increase in entrainment velocity could affect both convective heat transfer and species transport. Particularly for thin fuel elements this would alter the convective heat transfer coefficient and the resulting cooling during the pre-heating period. Similarly, the effect on oxygen supply and mixing within the combustion region requires further investigation, particularly given the observed variation in buoyant flow profiles as a result of changes in the fuel bed structure.

#### 4. Conclusions

As in previous studies, for flame spread through porous natural fuel beds in quiescent conditions (no wind, no slope), flame spread rate (along with HRR and flame height) was found to increase with independent increases in fuel loading or decreases in bulk density. Yet in terms of linking these bulk parameters to the physical processes driving flame spread, neither parameter alone can sufficiently explain the observed changes in fire behavior. A better correlation is observed with a dimensionless fuel bed parameter  $\alpha\sigma\delta$  in a similar manner to previous studies, particularly those involving cribs and engineered fuel beds.

Independent changes in bulk density and fuel loading were observed to result in variations in the buoyant flow profile. In the buoyancy controlled regime explored in this study, this buoyant flow drives lateral entrainment towards the fire front. Variations in the entrainment flow profile through the porous fuel bed were observed as this buoyant flow profile changed,

with an overall trend of increasing mean entrainment velocity towards the approaching flame front as the fuel loading (and hence HRR and buoyant flow velocity) increased. Variations in mean entrainment flow for fuel beds of different fuel loading, along with the variation between the mean and minimum entrainment velocity towards the approaching flame front, indicate the need to further quantify the role of bulk and local fuel bed structure and the subsequent changes in oxygen supply and convective heat transfer on the combustion region and the overall flame spread process.

## 5. Acknowledgements

The authors wish to thank the Strategic Environmental Research and Development Program (SERDP) for their financial support under the project grant RC-2641. The authors would also like to thank Hugo Rouvrais and Cameron Macleod for their assistance with the experiments.

## 6. References

- [1] J.L. Dupuy, J. Maréchal, Slope effect on laboratory fire spread: Contribution of radiation and convection to fuel bed preheating, *Int. J. Wildl. Fire.* 20 (2011) 289–307. doi:10.1071/WF09076.
- [2] C.E. Van Wagner, Fire behaviour mechanisms in a Red Pine plantation: field and laboratory evidence., Canadian Department of Forestry and Rural Development; Departmental publication 1229, 1968.
- [3] C.E. Van Wagner, Effect of slope on fires spreading downhill, *Can. J. For. Res.* 18 (1988) 818–820.
- [4] C.G. Rossa, D.A. Davim, D.X. Viegas, Behaviour of slope and wind backing fires, *Int. J. Wildl. Fire.* 24 (2015) 1085–1097. doi:10.1071/WF14215.
- [5] J.R. Raposo, S. Cabiddu, D.X. Viegas, M. Salis, J. Sharples, Experimental analysis of fire spread across a two-dimensional ridge under wind conditions, *Int. J. Wildl. Fire.* 24 (2015) 1008–1022. doi:10.1071/WF14150.
- [6] R.C. Rothermel, H.E. Anderson, Fire Spread Characteristics Determined In The Laboratory, US Forest Service Research Paper INT-30, 1966.
- [7] R.M. Nelson, Reaction times and burning rates for wind tunnel headfires, *Int. J. Wildl. Fire.* 12 (2003) 195–211. doi:10.1071/WF02041.
- [8] M.J. Gollner, C.H. Miller, W. Tang, A. V. Singh, The effect of flow and geometry on concurrent flame spread, *Fire Saf. J.* 91 (2017) 68–78. doi:10.1016/j.firesaf.2017.05.007.
- [9] W.R. Beaufaut, Characteristics of Backfires and Headfires in a Pine Needle Fuel Bed, US Forest Service Research Note INT-39, 1965.
- [10] J.-H. Balbi, D.X. Viegas, C. Rossa, J.-L. Rossi, F.-J. Chatelon, D. Cancellieri, A. Simeoni, T. Marcelli, Surface Fires: No Wind, No Slope, Marginal Burning, *J. Environ. Sci. Eng. A.* 3 (2014) 73–86. <https://hal.archives-ouvertes.fr/hal-01070946>.
- [11] F. Morandini, Y. Perez-Ramirez, V. Tihay, P.A. Santoni, T. Barboni, Radiant, convective and heat release characterization of vegetation fire, *Int. J. Therm. Sci.* 70 (2013) 83–91. doi:10.1016/j.ijthermalsci.2013.03.011.
- [12] R.A. Wilson, A Reexamination of Fire Spread in Free-Burning Porous Fuel Beds, US Forest Service: Research Paper INT-289, 1982.



- 490 [13] D. Morvan, Numerical study of the effect of fuel moisture content (FMC) upon the  
491 propagation of a surface fire on a flat terrain, *Fire Saf. J.* 58 (2013) 121–131.  
492 doi:10.1016/j.firesaf.2013.01.010.
- 493 [14] M.A. Finney, J. Forthofer, I.C. Grenfell, B.A. Adam, N.K. Akafuah, K. Saito, A study  
494 of flame spread in engineered cardboard fuelbeds: Part I: Correlations and  
495 observations, in: *Proc. Seventh Int. Symp. Scale Model.*, 2013.
- 496 [15] G.M. Byram, Forest fire behavior. *Forest Fire: Control and Use*, AA Brown and KP  
497 Davis, Eds, (1959).
- 498 [16] E.E. Zukoski, Properties of fire plumes, in: G. Cox (Ed.), *Combust. Fundam. Fire*,  
499 Academic Press, 1995: pp. 101–220.
- 500 [17] P. Joulain, The behavior of pool fires: State of the art and new insights, *Symp.*  
501 *Combust.* 27 (1998) 2691–2706. doi:10.1016/S0082-0784(98)80125-2.
- 502 [18] P.J. Pagni, T.G. Peterson, Flame spread through porous fuels, *Symp. Combust.* 14  
503 (1973) 1099–1107. doi:10.1016/S0082-0784(73)80099-2.
- 504 [19] X. Silvani, F. Morandini, J.L. Dupuy, A. Susset, R. Vernet, O. Lambert, Measuring  
505 velocity field and heat transfer during natural fire spread over large inclinable bench,  
506 *Exp. Therm. Fluid Sci.* 92 (2018) 184–201. doi:10.1016/j.expthermflusci.2017.11.020.
- 507 [20] W.R. Anderson, E.A. Catchpole, B.W. Butler, Convective heat transfer in fire spread  
508 through fine fuel beds, *Int. J. Wildl. Fire.* 19 (2010) 284–298. doi:10.1071/WF09021.
- 509 [21] A.C. Fernandez-Pello, S.R. Ray, I. Glassman, Flame Spread in an Opposed Flow: The  
510 Effect of Ambient Oxygen Concentration, *Symp. Combust.* 18 (1981) 579–589.  
511 doi:10.1016/S0082-0784(81)80063-X.
- 512 [22] J.L. Torero, A. Simeoni, Heat and Mass Transfer in Fires: Scaling Laws, Ignition of  
513 Solid Fuels and Application to Forest Fires, *Open Thermodyn. J.* 4 (2014) 145–155.  
514 doi:10.2174/1874396x01004010145.
- 515 [23] G.M. Byram, H.B. Clements, M.E. Bishop, R.M. Nelson Jr., *Project Fire Model - An*  
516 *experimental study of model fires: final report*, USDA Forest Service, Southeastern  
517 Forest Experiment Station, Southern Forest Fire Laboratory, Macon, Georgia., 1966.
- 518 [24] J.L. Dupuy, Slope and fuel load effects on fire behaviour :Laboratory experiments in  
519 pine needles fuel beds, *Int. J. Wildl. Fire.* 5 (1995) 153–164. doi:10.1071/WF9950153.
- 520 [25] P.A. Santoni, P. Bartoli, A. Simeoni, J.L. Torero, Bulk and particle properties of pine  
521 needle fuel beds – influence on combustion, *Int. J. Wildl. Fire.* 23 (2014) 1076–1086.  
522 doi:10.1071/WF13079.
- 523 [26] R.C. Rothermel, A Mathematical Model for Predicting Fire Spread in Wildland Fuels,  
524 USDA Forest Service. Research Paper INT-115, 1972.
- 525 [27] C.G. Rossa, P.M. Fernandes, Empirical modeling of fire spread rate in no-wind and no-  
526 slope conditions, *For. Sci.* 64 (2018) 358–370. doi:10.1093/forsci/fxy002.
- 527 [28] H.E. Anderson, Relationship of Fuel Size and Spacing to Combustion Characteristics  
528 of Laboratory Fuel Cribs, USDA Forest Service. Research Paper INT-424, 1990.
- 529 [29] S. McAllister, M. Finney, Burning Rates of Wood Cribs with Implications for  
530 Wildland Fires, *Fire Technol.* 52 (2016) 1755–1777. doi:10.1007/s10694-015-0543-5.

- [30] J.L. Dupuy, J. Maréchal, D. Portier, J.C. Valette, The effects of slope and fuel bed width on laboratory fire behaviour, *Int. J. Wildl. Fire.* 20 (2011) 272–288. doi:10.1071/WF09075.
- [31] M.L. Janssens, Measuring rate of heat release by oxygen consumption, *Fire Technol.* 27 (1991) 234–249. doi:10.1007/BF01038449.
- [32] P. Bartoli, Feux de forêt: amélioration de la connaissance du couplage combustible-flamme, [PhD Thesis], 2011.
- [33] B.J. McCaffrey, G. Heskestad, A robust bidirectional low-velocity probe for flame and fire application, *Combust. Flame.* 26 (1976) 125–127. doi:10.1016/0010-2180(76)90062-6.
- [34] F. Morandini, X. Silvani, L. Rossi, P.A. Santoni, A. Simeoni, J.H. Balbi, J. Louis Rossi, T. Marcelli, Fire spread experiment across Mediterranean shrub: Influence of wind on flame front properties, *Fire Saf. J.* 41 (2006) 229–235. doi:10.1016/j.firesaf.2006.01.006.
- [35] K.L. Clark, N. Skowronski, M. Gallagher, The fire research program at the Silas Little Experimental Forest, New Lisbon, New Jersey, USDA For. Serv. Exp. For. Ranges Res. Long Term. (2014) 515–534. doi:10.1007/978-1-4614-1818-4\_22.
- [36] T. Marcelli, P.A. Santoni, A. Simeoni, E. Leoni, B. Porterie, Fire spread across pine needle fuel beds: Characterization of temperature and velocity distributions within the fire plume, *Int. J. Wildl. Fire.* (2004). doi:10.1071/WF02065.
- [37] J.C. Thomas, R.M. Hadden, A. Simeoni, Experimental investigation of the impact of oxygen flux on the burning dynamics of forest fuel beds, *Fire Saf. J.* 91 (2017) 855–863. doi:10.1016/j.firesaf.2017.03.086.
- [38] F. Morandini, X. Silvani, J.L. Dupuy, A. Susset, Fire spread across a sloping fuel bed: Flame dynamics and heat transfers, *Combust. Flame.* 190 (2018) 158–170. doi:10.1016/j.combustflame.2017.11.025.
- [39] C.G. Rossa, The effect of fuel moisture content on the spread rate of forest fires in the absence of wind or slope, *Int. J. Wildl. Fire.* (2017). doi:10.1071/WF16049.

## List of Figures

- Fig. 1. Photograph and schematic of the Table, detailing the position of in-bed bi-directional pressure probes and gas phase thermocouples (all measurements at a height of 0.01 m above the vermiculite substrate surface)
- Fig. 2. Composite of frames from downward-looking video footage of flame spread experiments displaying variation in flame and front shape between Pitch Pine fuel beds of (Top) 0.2 kg/m<sup>2</sup>, 20 kg/m<sup>3</sup> (Middle) 0.8 kg/m<sup>2</sup>, 20 kg/m<sup>3</sup> (Bottom) 1.6 kg/m<sup>2</sup>, 20 kg/m<sup>3</sup>.
- Fig. 3. Flame front position versus time from ignition for Pitch Pine beds of (a) 20 kg/m<sup>3</sup> bulk density, and (b) 0.8 kg/m<sup>2</sup> fuel loading (avg. of all experiments at each condition)
- Fig. 4. Flame Spread Rate as a function of distance (based on video analysis) for Pitch Pine fuel beds of different fuel loadings at (a) 10 kg/m<sup>3</sup> bulk density, and (b) 20 kg/m<sup>3</sup> bulk density
- Fig. 5. Comparison of flame spread rate with fuel loading and bulk density for, (a) Pitch Pine (b) Pitch-Loblolly Pine hybrid, needle fuel beds
- Fig. 6. Correlation between  $\alpha\sigma\delta$  and flame spread rate in (a) Pitch Pine (b) Pitch-Loblolly Pine fuel beds
- Fig. 7. Comparison of (a) Fuel Loading, (b) Heat Release Rate with mean and max. buoyant flow velocity at a height of 1.2 m above Pitch Pine fuel bed, in the 10 s after flame arrival
- Fig. 8. Mean and minimum in-bed flow velocity towards the approaching flame front (50 mm to 10 mm prior to flame arrival), in beds of different fuel loading and bulk density for beds of Pitch Pine and Pitch-Loblolly Pine hybrid respectively

## Highlights:

- Neither fuel loading or bulk density, adequately describes the effect of porous fuel bed structure on flame spread.
- Existing dimensionless fuel bed descriptors can be adapted to describe pine needle fuel beds.
- Positive relationship between buoyant flow induced by the flame, and fuel loading.
- Increase in mean in-bed air entrainment with increasing fuel load.
- Effect of bed structure on both in-bed and above-bed flow quantified.